Electronic properties of α-UH_3 stabilized by Zr

I. Tkach,[1] M. Paukov,[1] D. Drozdenko,[1] M. Cieslar,[1] B. Vondráčková,[1] Z. Matěj,[1] D. Kriegner,[1] A.V. Andreev,[2] N.-T. H. Kim-Ngan,[3] I. Turek,[1] M. Diviš,[1] and L. Havela[1]

[1]*Faculty of Mathematics and Physics, Charles University, Ke Karlovu 5, 12116 Prague 2, Czech Republic*

[2]*Institute of Physics, Academy of Sciences, Na Slovance 2, 18221 Prague, Czech Republic*

[3]*Institute of Physics, Pedagogical University Cracow, Poland*

(Received 23 December 2014; published 6 March 2015)

Pure hydride of the α-UH_3 type without any β-UH_3 admixture was prepared by high-pressure hydrogenation of bcc U stabilized by Zr. Such material, characterized by a general formula $(UH_3)_{1-x}Zr_x$, is stable in air at ambient and elevated temperatures. H release is observed in the range of 400–600 °C similar to β-UH_3. Its stability allowed us to measure the magnetic properties, specific heat, and electrical resistivity in a wide temperature range. Despite the rather different crystal structure and inter-U spacing, the electronic properties are almost identical to β-UH_3. Its ferromagnetic ground state with Curie temperature $T_C \approx 180$ K (weakly and nonmonotonously dependent on Zr concentration) and U moments of 1.0 μ_B indicate why mixtures of α- and β-UH_3 exhibited only one transition. Magnetic ordering leads to a large spontaneous magnetostriction $\omega_s = 3.2 \times 10^{-3}$, which can be explained by the increase of the spin moment between the paramagnetic (disordered local moment) and the ferromagnetic states. The role of orbital moments in magnetism is indicated by fully relativistic electronic structure calculations.

DOI: 10.1103/PhysRevB.91.115116 PACS number(s): 65.40.−b, 71.20.−b, 75.30.−m

I. INTRODUCTION

The interaction of hydrogen with uranium is an important issue in the field of nuclear energy and weapons. Any contact with H is detrimental for mechanical integrity and in addition a very fine powder of uranium hydride tends to self-ignite if exposed to air [1]. On the other hand, uranium hydride provides a tool to observe the impact of expansion of the U lattice, allowing the formation of U moments and their ferromagnetic ordering.

Its stable allotropic form, β-UH_3, is a ferromagnet with magnetic moments $\mu \approx 1\,\mu_B$/U [2]. Its magnetic ordering contrasts with the Pauli paramagnetic behavior of U metal, which has a low magnetic susceptibility $\chi \approx 5.0 \times 10^{-9}$ m^3/mol for the orthorhombic α-U form [3]. The difference can be qualitatively ascribed to the enhanced U-U spacing in the hydride, which yields a $5f$-band narrowing, necessary for fulfillment of the Stoner criterion. The crucial role of the $5f$-$5f$ spacing in determination of the ground state (magnetic contra superconducting) was recognized by Hill [4], who besides U drew similar systematics for Ce, U, and Pu compounds. At present, it is evident that the occurrence of magnetic order in Ce compounds is primarily affected by the Kondo physics (depending on the $4f$ hybridization with ligand states [5]), while more complicated many-body effects and the fine balance between $5f^5$ and $5f^6$ are primary in Pu systems [6,7]. Nevertheless, the U and Np alloys and compounds are assumed to be depending on the An-An spacing $d_{An\text{-}An}$. The $5f$-ligand hybridization as a possible second delocalization mechanism [8] (besides the direct $5f$-$5f$ overlap), becomes prominent for large $d_{An\text{-}An}$. The critical value $d_{An\text{-}An}$ for U, which should be taken with some spread, is assumed around 340 pm. β-UH_3 with $d_{An\text{-}An} = 330$ pm must be therefore somewhere just at the real minimum distance. One can compare, for example, with $d_{An\text{-}An} \approx 300$ pm for γ-U, which is as weakly paramagnetic as α-U [9]. It is, however, surprising that a compound close to the verge of magnetism can have a relatively high Curie temperature $T \approx 170$ K. Ferromagnetism at such $d_{An\text{-}An}$ is more typical than antiferromagnetism, which prevails at $d_{An\text{-}An} > 400$ pm, but T_C over 100 K can be found only in cases like UGa_2 ($T_C = 126$ K) with much higher U moments, which can develop due to large $d_{An\text{-}An} = 401$ pm. Other U compounds in the range of the Hill limit have, if ferromagnetic at all, much lower T_C values [10].

The cubic structure of β-UH_3 can apparently accept some doping. It was found, by hydrogenating U_6Fe, that one of the U positions can accept Fe atoms [11], yielding U_6FeH_{17} [corresponding to $(UH_{\approx 2.8})_{0.86}Fe_{0.14}$]. The resulting Curie temperature 173 K practically coincides with that of β-UH_3. Conspicuously similar $T_C = 185$ K was reported for U_6CoH_{18} formed in the same structure [12].

An interesting comparison is offered by the existence of α-UH_3, which forms as metastable in the early stage of hydrogenation and transforms fast at elevated temperatures into β-UH_3 [13]. The latter has the Cr_3Si structure type, there are 2 different U sites, and the H atoms occupy distorted tetrahedral insterstitials. The cubic unit cell is large ($a =$ 664 pm), containing 8 f.u., and the H positions depend on internal structure parameters. The cubic unit cell of α-UH_3 is smaller (416 pm), contains only 2 f.u., H atoms adopt the Cr positions, and there are no internal parameters [14]. The U sublattice represents the bcc lattice, it can be therefore taken as an expanded γ-U structure (70% volume expansion).

The fact that α-UH_3 was never studied in a pure form but always in a mixture with β-UH_3 is a reason of uncertainty as to the type of ground state. While earlier works, reviewed in Ref. [2], deduced magnetic ordering with T_C coinciding with that of β-UH_3, in a later neutron diffraction work it was identified as nonmagnetic [15]. That would seriously contradict to the concept of the U magnetism depending on the $5f$-$5f$ overlap. The density of α-UH_3 (11.12 g/cm^3) is slightly higher than for β-UH_3 (10.92 g/cm^3), but the shortest U-U spacing 360 pm is considerably larger than 330 pm for β-UH_3. It is therefore strongly desirable to clarify the basic electronic properties of α-UH_3.

We undertook a hydrogenation study of γ-U phases doped by Mo or Zr, which helps to retain the bcc structure to low

temperatures. Both types of alloys are very stable with respect to hydrogen, and high H_2 pressures are needed to form a hydride. While the Mo doping leads to amorphized hydrides of the β-UH_3 type [16], we found that the Zr doping leads to a stable single phase α-UH_3 type of hydride, which opens an avenue for investigation of basic magnetic, transport, and thermodynamic properties. In the present work, the magnetic and magnetoelastic properties of α-UH_3 as well as the Sommerfeld coefficient γ are experimentally determined. A deeper insight into the electronic properties is provided by different types of electronic structure calculations, which reveal an important role of orbital magnetic moments, which are necessary to explain phenomena originating from high magnetic anisotropy.

II. MATERIALS SYNTHESIS AND EXPERIMENTAL METHODS

Starting $U_{1-x}Zr_x$ alloys were prepared by arc melting of pure elements (U-2N8, Zr-3N) in argon atmosphere using an arc furnace. Each ingot was turned and remelted 3 times for better homogenization of constituents. Because the alloys are not in the range of thermodynamic stability of the bcc structure (γ-U), we used ultrafast (splat) cooling to ensure the phase homogeneity. Another advantage of samples produced by splat cooling, which are in fact foils about 100-μm thick, is that the shape allows taking an x-ray diffraction pattern from the surface. The alloys are otherwise hard and cannot be crushed into a powder. The XRD study, performed using the Bruker D8 Advance diffractometer with Cu K_α radiation, indicated the bcc structure plus a small amount of impurities (ZrC and UO_2), residing mostly at the surface. The lattice parameters are listed in Table I. Pure U splats used for comparison exhibit the α-U structure.

Additional phase purity analysis was done by means of x-ray energy dispersive microanalysis (EDX) using the scanning electron microscope (SEM) FEI Quanta 200 FEG. The surface was prepared by mechanical polishing, followed by Ar ion gun bombardment using the voltage 4 kV.

For higher Zr concentrations, the ultrafast cooling is not necessary, and normal cooling in the arc furnace is sufficient to retain the single-phase bcc structure. Therefore we could alternatively work further on with ingots. In this case, the XRD study was not performed; the lattice parameters are therefore not included in Table I. The sample with 40% Zr concentration exhibited an inhomogeneous Zr distribution in the bulk form; it was therefore excluded from further study.

For the hydrogenation, the samples were placed in an alumina crucible into a reactor, which could be pressurized to 150 bar of H_2. The reactor was first evacuated down to 10^{-6} mbar and then H_2 gas was introduced. We found that minimum H_2 pressure for the hydride formation is, irrespective of composition, in the range 4–5 bars. Higher pressures (up to 100 bar) can only fasten the process, but the H amount absorbed remains the same. As lower pressures allow better monitoring of the process (by recording pressure variations in a closed volume) and its completion, we used as a standard the H_2 pressure of 5 bar.

The desorption in a closed evacuated volume was performed with the temperature ramping 2 K/min. As all H is released from β-UH_3 at 450 °C, we took 800 °C as an upper limit. We typically observed a release in the range 400–600 °C in two close steps, which we assign to two competing processes proceeding at very similar temperatures. H is either released from the ternary hydride, or Zr segregates, leaving β-UH_3, which releases H_2 in the next step. As $U_{1-x}Zr_x$, which would be left in the first case, decomposes at 500 °C into UZr_2 and α-U, the final products are the same in both cases.

The total amount of H_2 released corresponds to approximately 3 H atoms per 1 U atom (see Table I). Therefore we adopted the formula $(UH_3)_{1-x}Zr_x$. The uncertainty as to the H concentration is affected by the fact that it has to be determined from the pressure increase in a closed system, which is not all at the same temperature. Cooling the reactor (i.e., the hot part of the system) to room temperature leads to a reabsorption of the gas, presumably by the α-U phase.

The hydride samples were subsequently crushed and subjected for further structure characterization by x-ray powder diffraction. The Physical Property Measurement System (PPMS) equipment was used for magnetization and specific heat measurements, preformed in the temperature range 2–300 K and in magnetic fields up to 14 T. For the specific heat measurements, the samples were in the form of powder pressed to make a pellet. The magnetization was measured on powder samples with grains glued in a random orientation. One of the hydride samples, $(UH_3)_{0.85}Zr_{0.15}$, consisted of elongated fragments 2–3 mm large, which allowed to attach electrical contacts by a silver paste and measure the temperature dependence of electrical resistivity, also using the PPMS system.

III. RESULTS

A. Crystal structure

XRD patterns of the $(UH_3)_{1-x}Zr_x$ hydrides are presented in Fig. 1. In contrast with the Mo doped hydrides studied previously [16,17], the XRD patterns for the Zr doped hydrides reveal a crystalline state, which is clearly different from β-UH_3. A closer inspection indicated a bcc structure,

TABLE I. Room-temperature lattice parameter a, H concentration, paramagnetic Curie temperature Θ_p, Curie temperature T_C, spontaneous magnetization M and Sommerfeld coefficient of electronic specific heat γ for hydrides of various $U_{1-x}Zr_x$ alloys.

Compound	a (pm) precursor	a (pm) - hydride	H conc. (at./U)	Θ_p (K)	T_C (K)	M (μ_B/U)	γ (mJ/molU K^2)
$U_{0.89}Zr_{0.11}$-H	354.2	416.1	–	177	174	1.03	31.4
$U_{0.85}Zr_{0.15}$-H	353.8	414.3	2.8(2)	187	186	0.90	–
$U_{0.80}Zr_{0.20}$-H	356.0	414.3	2.8(2)	181	167	1.02	32.2
$U_{0.70}Zr_{0.30}$-H	354.3	414.2	2.7(3)	184	163	0.85	–

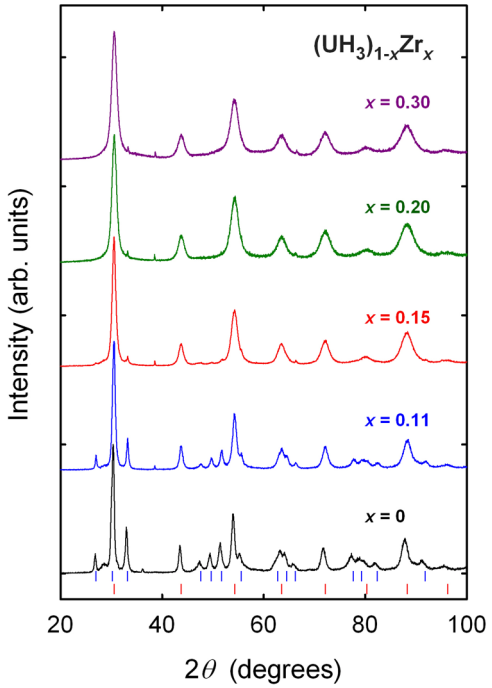

FIG. 1. (Color online) X-ray diffraction pattern of the $(UH_3)_{1-x}Zr_x$ hydrides. The ticks indicate positions of diffraction lines expected for α-UH_3 (red ticks - lower line) and β-UH_3 (blue ticks - upper line). In addition, weak lines of ZrH_2 can be distinguished.

which is very much expanded (by 75% in volume expansion) with respect to the bcc precursors. The lattice parameters $a \approx 416$ pm are very close to the known α-UH_3 structure (Table I). A small amount of ZrC impurity was also observed from diffraction patterns for all hydrides. A small amount of ZrH_2 is not excluded for higher Zr concentrations. Hydride prepared from the pure U splat shows a mixture of β-UH_3 and α-UH_3 phases, with β-UH_3 as the dominant phase. Adding Zr, the concentration of α-UH_3 phase increases, while the concentration of β-UH_3 decreases. For $x = 0.15$, only tiny peaks of residual β-UH_3 could be recognized. For $x \geqslant 0.20$, no β-UH_3 can be observed. The peak broadening indicates a grain size in the range 10–20 nm.

The XRD study was repeated after investigations of physical properties, i.e., after one month mostly at room temperature. The samples with low Zr concentration exhibited some changes. The α-UH_3 phase in pure-U hydride and $(UH_3)_{0.89}Zr_{0.11}$ has been partly transformed to UO_2. No significant changes have been observed by XRD for samples with higher Zr concentrations.

B. Magnetization

As an example, we display (Fig. 2) the temperature dependence of magnetization of $(UH_3)_{0.80}Zr_{0.20}$, which has undoubtedly the single phase of the α-UH_3 type. Measurements in various fields indicate ferromagnetism below $T \approx 175$ K, leading to spontaneous magnetization of $\approx 1.0\ \mu_B$/U. A closer inspection of $M(T)$ dependence in the ordered state reveals that magnetization is not smoothly increasing with decreasing T, as usually in ferromagnets, instead a flat part appears around 45 K, with possible slight decreases with further reducing T.

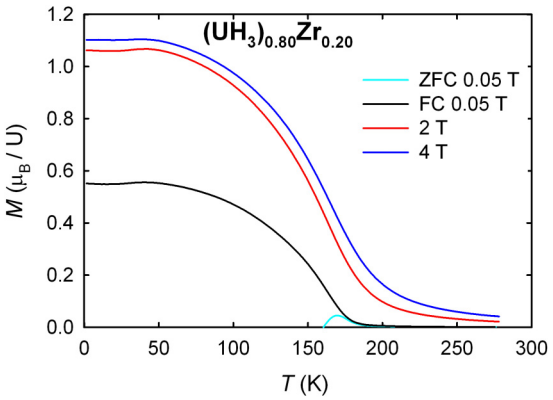

FIG. 2. (Color online) Temperature dependence of magnetization of $(UH_3)_{0.80}Zr_{0.20}$ measured in various magnetic fields. Measurements for $\mu_0 H = 0.05$ T were performed in the field-cooled (FC) and zero-field-cooled mode (ZFC), the latter exhibiting a very weak response except in the temperature range in the vicinity of T_C.

One has to stress that all the T dependencies were measured in the field-cooling mode. This effect can be perhaps attributed to a high anisotropy, progressively increasing with decreasing T, which forces some of the moments from the field direction towards easy magnetization directions. Alternatively, one may consider that some antiferromagnetic components of exchange coupling (leading to noncollinear moments) develop at low temperatures, perhaps in relation with the variable U-U spacing introduced by the Zr doping.

The weak decrease of magnetization with decreasing T can be observed also on hysteresis loops, obtained for the same sample [Figs. 3(a) and 3(b)], using the field sweeping rate 0.0045 T/s in the range from -1 to 1 T and 0.009 T/s outside this range. The prominent feature of the loops is that they do not reach the reversible behavior even in $\mu_0 H = 12$ T. At this stage we can only speculate about details of magnetization processes, which can be very complicated for nanostructured inhomogeneous ferromagnets. We can expect single domain grains of high and random anisotropy, but as deduced in Ref. [18], they are exchange-coupled into larger interaction domains. The remagnetization happens in many grains in the same time, which can explain the magnetization jumps observable at the lowest temperatures (1.8 and 3 K). Their smearing at higher T reflects relatively easy thermally assisted excitation. Similar jumps also appear in the case of pinning of narrow domain walls. As shown, e.g., for rare-earth compounds with transition metals, randomness on the transition-metal sublattice with relatively small magnetic moments yields a fundamental coercivity due to fluctuations of exchange interactions or anisotropy, which stabilize domain walls in given positions. The coercive field decrease follows the $-aT^{1/2}$ dependence deduced by the Egami model of thermally activated movements of domain walls [19]. Similar to the Egami model, it deviates from this dependence and saturates at low temperatures. One should notice that the smooth demagnetization curve turns into large erratic steps, corresponding to re-magnetization avalanches. We use this word for stressing a kinetic effect, leading to a faster demagnetization even if T is lower when the avalanche is triggered comparing to somewhat higher temperatures with smooth thermally assisted motion.

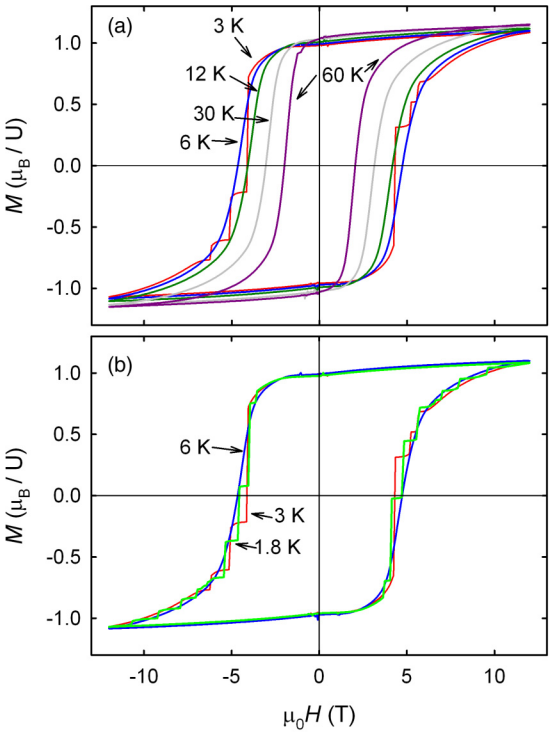

FIG. 3. (Color online) Hysteresis loops of $(UH_3)_{0.80}Zr_{0.20}$ measured at various temperatures. The panel (a) covers higher temperatures, the panel (b) compares the lowest temperatures, revealing how the smooth behavior of the magnetization changes into erratic steps below $T = 6$ K.

Although the phenomenology is very similar, e.g., to $SmCo_{1.4}Ni_{3.6}$ [20], in the U-Zr hydrides we consider the dilution of the U sublattice by Zr introducing "defects" in the exchange interaction and/or anisotropy. The most essential prerequisite of the model, the large anisotropy, is inherent to $5f$ itinerant systems. The strong magnetic anisotropy is traditionally associated with crystal-field phenomena of localized $4f$ states in lanthanides. In light actinides, where the $5f$ states are part of metal bonding, and the strong spin-orbit interaction induces large orbital moments, an anisotropy of a different type is encountered, which is related to the directionality of the $5f$-$5f$ bonding. This so-called two-ion anisotropy, whose energy can be of the order of several hundred Kelvin, is particularly noticeable in low-symmetry structures [21], but can be expected even in cubic materials. The central idea is that when the involvement of the $5f$ into bonding is directional, it leads to a population of the $5f$ states with orbital moments perpendicular to the strong bonding directions. The mechanism of such an anisotropy was deduced from the moment directions even for weak ferromagnets with $d_{U\text{-}U}$ far below the Hill limit, such as UNi_2 or U_2Fe_3Ge [22].

The magnetic hardness even increases with more Zr doping, reaching $\mu_o H_c = 6$ T for $(UH_3)_{0.70}Zr_{0.30}$. The T-dependence type remains the same. Using the relation $H_c(T)/H_c(0) = 1 - \eta T^{1/2}$ [19] we obtain the same value of $\eta = 0.082\,\mathrm{K}^{-1/2}$ for both Zr concentrations. As seen from Fig. 4, the two-phase hydride with $(UH_3)_{0.89}Zr_{0.11}$ has the η value smaller.

Naturally, the primary interest is the variation of T_C and μ_s with the Zr concentration. The values of Curie temperature

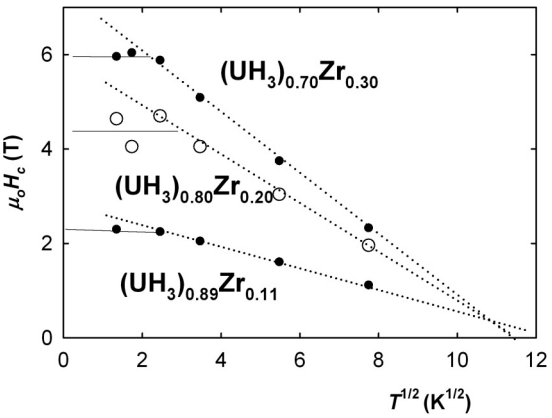

FIG. 4. The values of the coercive field for the hydrides $(UH_3)_{1-x}Zr_x$ obtained from the hysteresis loops follow the scaling of the 1-$\eta T^{1/2}$ type in the high-T part.

were determined for each sample by several methods, using either the inflexion point of $M(T)$ in low magnetic fields or by the Arrott plots (M^2 versus H/M dependencies for temperatures bracketing the expected T_C value), or the T dependence of the specific heat, $C_p(T)$. One can notice a certain increase of T_C for low Zr concentrations up to $T_C = 186$ K (see Table I and Fig. 5), which is reminiscent of the increase in Mo-doped UH_3 [16]. Neither Zr nor Mo belong to traditional "magnetic" elements, but there are cases [as $(U,Y)B_4$] in which a small dilution can induce magnetic order [23]. In general, one can consider variations of the mean U-U spacing or changing the balance of conduction electrons, or a combination of both responsible. Magnetic moments per 1 U atom deduced from $M(H)$ at low temperatures do not show any real tendency, being on the level of 0.9 μ_B/U (see Table I).

The dilution of an active magnetic sublattice leads typically to a broadening of the transition, as seen in magnetization, and apparently it is the case even here. For low Zr concentrations, it is the two-phase nature that can also produce a broadening. The result is the relatively large error bars displayed in Fig. 5. We can, however, conclude a very weak Zr concentration dependence of T_C, which is different than effects of the $5f$ dilution in regular band U-based ferromagnets, such as U(Th,Lu)RhAl, in which the long-range order vanishes

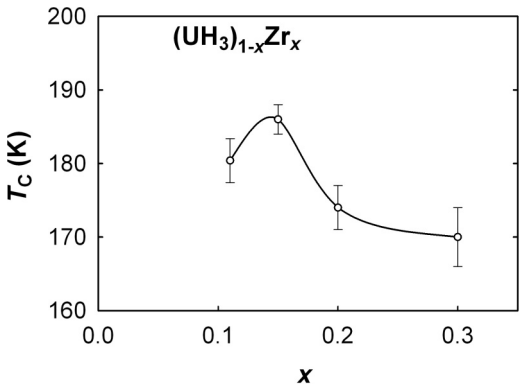

FIG. 5. Concentration dependence of the Curie temperature for the hydrides $(UH_3)_{1-x}Zr_x$. The full line is a guide to the eye.

entirely for 15% Lu or 35% Th (the difference between the two is likely a volume effect related to much larger Th atoms) [24]. Thus, besides the increase of T_C, it is mainly the lack of suppression of the $5f$ magnetism with doping, which seem unusual and which suggest that the UH_3-based hydrides are not just usual $5f$-band ferromagnets. Practically constant spontaneous moments and even similar variations of T_C resemble more the local-moment materials (please do not confuse with localized $5f$ states) as (U,Th)CoSn, in which the moments decrease dramatically only close to the dilution limit [25].

The slow saturation of $M(H)$ dependencies makes also the derived values of spontaneous moments less accurate than usual. From the field dependence (up to 14 T) at $T = 1.8$ K, an estimate of the saturated moment can be done assuming a phenomenological relation $M(H) = M_s[1 - a/H^2] + \chi_{hf} H$, where the last term is accounting for the influence of field on the size of individual moments, while the first one accounts for the influence of anisotropy. The values obtained given in Table I are similar to β-UH_3 (with approx. 0.9 μ_B/U) and somewhat smaller than those that can be reached in $(UH_3)_{1-x}Mo_x$ [$M_s = 1.15\,\mu_B$/U in $(UH_3)_{0.85}Mo_{0.15}$]. All those values are therefore quite similar and far below the ionic moments ($\approx 3.2\,\mu_B$ for f^2 or f^3), which is in line with the strongly itinerant magnetism of the U hydrides. One should keep in mind that both spin and orbital components of total moments can differ from the free-ion prediction and they tend to orient antiparallel to each other in U compounds.

Magnetic susceptibility in the paramagnetic range (230–300 K) can be fitted by the Curie-Weiss law, $\chi = C/(T - \Theta_P)$, giving the effective moment normalized per U atom $\mu_{eff} = (2.2 \pm 0.1)\,\mu_B$/U. The paramagnetic Curie temperature Θ_P reaches (187 ± 2) K for $(UH_3)_{0.85}Zr_{0.15}$ and weakly decrease for higher Zr concentrations (see Table I). The parameters are practically independent of the Zr concentration within the experimental accuracy. The Θ_P values are comparable with literature data for β-UH_3 or β-UD_3 (168–181 K), the μ_{eff} values are slightly lower than typical literature data (2.2–2.4 μ_B/U). (For detailed summary of numerous studies one can consult Ref. [14].)

C. Specific heat

The temperature dependence of specific heat, $C_p(T)$, has not been studied systematically for all samples over the whole temperature range, which would include both the low-T and high-T behavior. For Curie temperatures almost 200 K, the magnetic part of the specific heat is only a small fraction of the lattice part, which together with experimental uncertainties (e.g., due to the subtraction of specific heat of Apiezon mediating the thermal contact) and rather smeared (due to an inhomogeneity related to U dilution) anomaly at T_C (see Fig. 6) brings us to a situation in which very little can be concluded about the magnetic specific heat itself. Comparing to the sharp anomaly for β-UH_3, we can deduce a spread of a part of magnetic entropy towards higher temperatures.

Figure 6 gives an example of $C_p(T)$ for $(UH_3)_{0.89}Zr_{0.11}$ and $(UH_3)_{0.70}Zr_{0.30}$ compared with $U_{0.70}Zr_{0.30}$ and β-UH_3, the last showing a sharp cusp related to T_C. The alloy $U_{0.70}Zr_{0.30}$ exhibits a Debye-type saturation, Θ_D is estimated as 160–170 K from the $C_p/T = \gamma + \beta T^2$ plot at low temperatures,

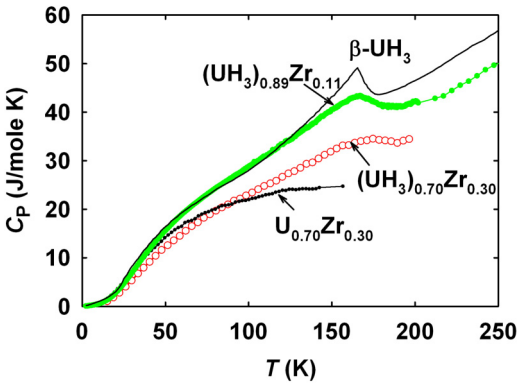

FIG. 6. (Color online) Temperature dependence of specific heat of selected hydrides $(UH_3)_{1-x}Zr_x$ compared with β-UH_3 [11] and $U_{0.70}Zr_{0.30}$.

using the relation $\beta = 1944/\Theta_D^3$ for C_p in J/mol K divided by the number of atoms in 1 mole.

Metal hydrides have typically a lattice specific heat that is affected by the Einstein vibration modes of the H atoms. As a result, a non-Debye character of $C_p(T)$ can be expected. However, an effective Debye temperature 280–310 K can be derived from the low-T slope of the plots for all hydrides $(UH_3)_{1-x}Zr_x$. These values are not far from $\Theta_D = 270$ K mentioned for β-UH_3 in Ref. [26].

The difference of the Debye temperatures between alloys and their hydrides may look surprising considering very similar behavior of $C_p(T)$ at low temperatures, from where the values are determined. The difference is a natural consequence of the normalization of the β-value per 1 atom—if H atoms are included in the balance, the slope per 1 atom decreases.

The similarity of the low-T part gives an alternative view of the lattice specific heat. The low-lying phonon modes (acoustic) are similar for the alloys and hydrides. The vibrations related to H atoms are characterized as high energy optical modes, revealed only at higher temperatures. Those were indeed observed by neutron scattering in the energy range 80–160 meV [27]. Only after the optical modes are populated, one can reach the classical limit for specific heat $3RN$ (N is the number of atoms in formula unit), which should be in the range 75–100 J/mol K, depending on the actual concentration of H. For UH_3, it is 99.8 J/mol K. The high energy of the optical modes is the reason why the experimental C_p values are below this limit still at $T = 250$ K.

The γ coefficient of low-temperature specific heat, which reflects the density of states at the Fermi level, $N(E_F)$, weakly increases with increasing Zr concentration, if normalized per mole of U. This normalization makes sense as the $5f$ states should be the main contributor to $N(E_F)$. Our analysis shows that the γ values change from 31.4 mJ/mol U K^2 for 11% Zr to 32.2 mJ/mol U K^2 for 20% Zr. On the other hand, considering that Zr and mainly its $4d$ states can contribute to the γ value, we may get approximately a constant, or even weakly decreasing, contribution of U if we, e.g., use the experimental value of γ for the Zr metal, 2.8 mJ/mol K^2. All values are very similar to those for pure β-UH_3 values presented in literature (29 mJ/mol K^2 [28] or 33.9 mJ/mol K^2 [29]). This underlines an important (but not well understood) fact, that

α- and β-UH_3 are almost identical not only as to magnetism, but also from the point of view of the density of electronic states at the Fermi level in the ferromagnetic state.

D. Electrical resistivity

The temperature dependence of electrical resistivity, $\rho(T)$, of β-UD_3 was determined using a compact sample synthesized at high temperatures and very high pressures, which helped to avoid fragmentation [26]. $\rho(T)$ can be seen as highly anomalous for a system with metallic conductivity, as it reaches 600 $\mu\Omega$cm in the paramagnetic state. Although such high absolute value can bring doubts about the geometrical factor (existence of cracks or voids), here we have to assume, considering the very low residual resistivity ρ_0, that the values are indeed realistic. Both the unrealistic geometrical factor and problems with metallicity (a low concentration of conduction electrons) would necessarily increase ρ_0. As the T_C anomaly is very pronounced and $\rho(T)$ is almost flat above T_C, we have to associate a large part of total resistivity (i.e., several hundred $\mu\Omega$cm) with spin-disorder scattering. It implies large U spin moments and a strong coupling of U spins, existing even in the paramagnetic state, to conduction electrons.

The $\rho(T)$ dependence of the γ-U alloys with Zr (not shown here) is similar to other bcc U alloys with, e.g., Mo [9]. The atomic disorder leads to a large increase of ρ_0 up to $\approx$100 $\mu\Omega$cm and the resulting nonadditivity of electron-phonon scattering gives an overall flattening of $\rho(T)$, and even a weak negative slope due to a weak localization. Reference [16] shows that $(UH_3)_{0.85}Mo_{0.15}$ combines flat $\rho(T)$ with a weak negative slope with very high absolute values, about 1 mΩcm (see inset of Fig. 7), with superimposed T_C anomaly in the form of a sharp but weak cusp, below which $\rho(T)$ resumes an increase with decreasing T. This suggests that a spin disorder contribution does not decrease below T_C, probably because the crystallographic disorder induces a strong magnetic disorder on the state characterized by bulk ferromagnetism.

$(UH_3)_{0.85}Zr_{0.15}$ behaves differently. Figure 7 demonstrates that resistivity drops below T_C with ρ_0 corresponding to 50% of the high T values. Cycling of temperature increases the resistivity value, which may be the impact of thermal expansion and spontaneous magnetostriction, described in the next paragraph, which open cracks in the brittle material, changing the effective geometrical factor. The anomaly related to T_C appears only as a knee, which is less pronounced than that for β-UH_3 [26], and which is further broadened and shifted somewhat to higher temperatures in the applied field $\mu_0 H = 3$ T, applied when the sample was at $T = 300$ K. The 3-T data reveal a similar irreversibility due to additional cracks opening, whose character remains similar to the zero field data, as seen when comparing with the 0 T heating data, normalized to the residual resistivity of the 3-T data (upper curve in Fig. 7). Both data sets exhibit the quadratic T dependence of resistivity up to $\approx$140 K.

E. Spontaneous magnetostriction

The temperature dependence of the lattice parameter a was measured in the temperature range 10–300 K using x-ray diffraction. Results are presented in Fig. 8 together with data published for β-UH_3 [26]. Our data set, which has a much lower scatter, reveals the similar expanding tendency, starting below $T \approx 200$ K, and leading to a pronounced invar effect, i.e., a compensation of the decreasing lattice volume with decreasing T by an expansion due to a magnetic contribution. The latter has to be associated with spontaneous magnetostriction, i.e., the volume expansion due to magnetic ordering. The size of magnetostriction can be estimated if we assume that a regular lattice thermal expansion, which is followed in the paramagnetic state, can be extrapolated down to $T = 0$ K. Using a Debye type of lattice expansion, used in Ref. [26] [the effective Debye temperatures for β-UH_3 and $(UH_3)_{1-x}Zr_x$ are quite similar], we obtained the spontaneous volume magnetostriction $\omega_s = 3.2 \times 10^{-3}$. This value is even higher than that estimated for β-UH_3, 2.7×10^{-3}, [26] and

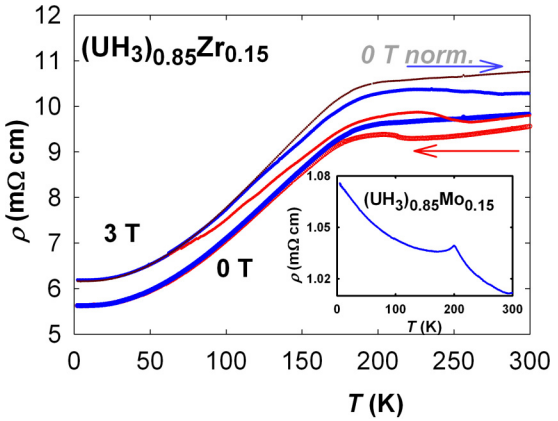

FIG. 7. (Color online) Temperature dependence of electrical resistivity of $(UH_3)_{0.85}Zr_{0.15}$ measured when cooling down (red) and heating up (blue) in zero field (thick line) and in applied field $\mu_0 H = 3$ T (thin line). The upper line represents the 0 T data with heating, renormalized to match the residual resistivity of the 3 T data. For comparison, resistivity data on $(UH_3)_{0.85}Mo_{0.15}$ are displayed in the inset.

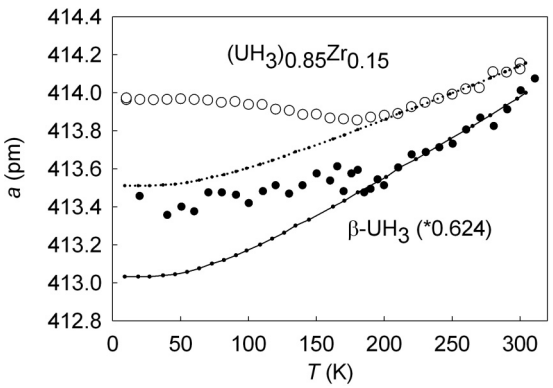

FIG. 8. Temperature dependence of the lattice parameter of $(UH_3)_{0.85}Zr_{0.15}$ compared with β-UH_3, (from Ref. [26]) with an extrapolated dependence from the paramagnetic state. The data on β-UH_3 are rescaled to match approximately those of $(UH_3)_{0.85}Zr_{0.15}$, which allows to compare mutually the magnetostriction and thermal expansion.

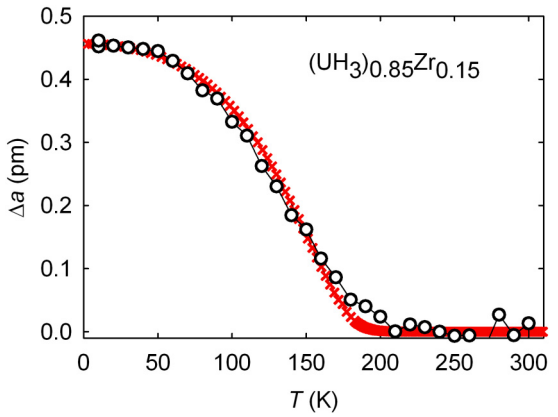

FIG. 9. (Color online) Temperature dependence of the lattice parameter a with the nonmagnetic contribution subtracted (the background in Fig. 8, empty circles). The red crosses correspond to M_s^2, both normalized arbitrarily to fit into the figure.

represents a truly remarkable value among the $5f$ systems. It is interesting to compare the effect with the temperature dependence of magnetization. Figure 9 displays the magnetic contribution, separated using the tentative background from Fig. 8. Using the spontaneous magnetization M_s estimated as $M_{4T} - 2M_{2T}$, we see that the volume effect follows well M_s^2, as expected for itinerant magnets. On the other hand, it gives a support to the background used. The data allow to determine also the coefficient of thermal expansion of $(UH_3)_{0.85}Zr_{0.15}$, $\alpha_v = 21 \times 10^{-6}\,K^{-1}$.

F. Electronic structure calculations

The first theoretical analysis of the electronic structure (using the APW method) was performed by Switendick [30], who noticed that the properties of α- and β-UH_3 may be very similar despite different U-U spacing. The suggestion that the U-U interaction is not as important as the U-H interaction seems to be right, although the work does not provide reliable details of the situation of $5f$ states. More recent scalar relativistic computations of UH_3 (both for the α and β forms) using the VASP package [13,31] reveal a mixed ionic and covalent bonding, while the latter becomes more important at small volumes and for the U (II) sites in β-UH_3, which have a lower U-U spacing. Although the equilibrium lattice parameters are well reproduced in the calculations, there remains a large disagreement as to the equilibrium bulk modulus B_0, which was calculated as 104 GPa for α-UH_3 and 144 GPa for β-UH_3, while the only experimental data [32] indicate a much softer lattice with $B_0 = 33 \pm 5$ GPa for β-UH_3. The value of B_0 does not change considerably even if LDA+U type of calculations are used [33]. The experimental value of B_0 for α-UH_3 is unknown.

In the present work, we decided to employ fully relativistic calculations including the spin-orbit interaction to assess to which extent basic magnetic properties (U ordered magnetic moments) can be reproduced assuming band magnetism. In addition, disordered local moment calculations were used to calculate moments in the paramagnetic state, which allows to assess spontaneous magnetostriction effects, obtained as a

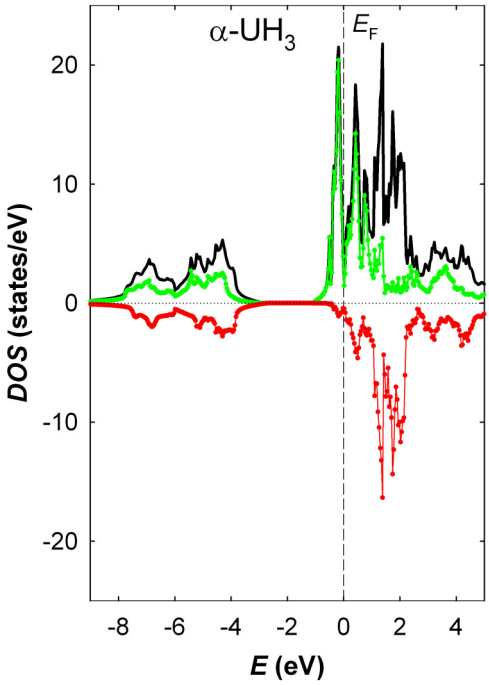

FIG. 10. (Color online) Total (black) and spin-resolved (green and red) density of states for α-UH_3 calculated using fully relativistic FPLO method.

difference between equilibrium volumes in ordered ($T = 0$ K) and disordered paramagnetic states. The same method was used to describe the effect of disorder imposed by random Zr substitution.

First, we used the full potential local orbitals code (FPLO) [34] applied on α-UH_3. This code solves the Dirac equation in the framework of density functional theory, local spin density approximation, using the widely used Perdew and Wang exchange-correlation potential [35]. At the experimental volume of α-UH_3, we found almost a complete compensation of large spin $M_S = 2.7\,\mu_B$ and orbital $M_L = -2.72\,\mu_B$ magnetic moments. The density of states is displayed in Fig. 10. Magnetic moments of hydrogen were negligible. We assume that the cancellation of both moments is accidental; the values of spin and orbital components in our calculations are considerably volume dependent (both components decrease with decreasing volume). The equilibrium volume of our particular local spin density approximation (LSDA) calculations for α-UH_3 comes out 9% higher ($a = 426$ pm) than the experimental one. At this volume, the orbital moment dominates over the spin moment already, while the total moment of $0.4\,\mu_B$/U is still too small comparing with experiment. The calculated total energies versus volume were fitted by Murnaghan equation of state. The obtained bulk modulus $B_0 = 101$ GPa is similar to all calculations mentioned above, and exhibits therefore a similar discrepancy with the experimental report of Halevy *et al.* [32].

Occupancies of individual states (Table II) for α-UH_3 compared with hypothetic bcc U of the same lattice parameter $a = 414$ pm indicate that H in a compound with strongly electropositive elements like U behaves electronegatively. Its occupancy increases from 1.0 to 1.74. This leads to the

TABLE II. Site projected occupancies of individual states for α-UH_3 (at experimental lattice parameter) and bcc U with the same lattice parameter. Occupancies of particular states in interstitial areas are not included.

State	α-UH_3	bcc U
U-6*d*	0.63	1.22
U-7*s*	0.03	0.42
U-5*f*	2.71	2.62
H-1*s*	1.74	

depletion of the U-7*s* states, while the U-6*d* states lose about 50% of their occupancy. The 5*f* states are affected very little, in fact, their occupancy slightly increased in our calculations. The almost complete loss of U-7*s* electrons and the partial depopulation of U-6*d* states can be taken to be responsible for the high values of electrical resistivity. H-1*s* states, although occupied by more than one electron, typically, form states separated from the Fermi energy by several eV and cannot contribute to the charge transport. Such situation with the 6*d* states shifted up in energy reduces the 5*f*-6*d* hybridization and supports the formation of ordering of the 5*f* magnetic moments.

The density of states (Fig. 10) for the experimental volume corresponds qualitatively to those given in Ref. [31] for the magnetic state, with almost all occupied 5*f* states only in the spin-up sub-band. A large gap between -1 and -3 eV separates the states in the Fermi level region from the density between -3 and -9 eV, which should contain the occupied H-1*s* states. The calculated Sommerfeld coefficient of the electronic specific heat $\gamma = 7.42\,\mathrm{mJ/mol\,K^2}$ is by a factor of 4 lower than the experimental value. The discrepancy may originate in the many-body effects not included in the LSDA method. The other reason may be in the fact that the Fermi level is located in the deep narrow minimum of DOS in our calculations. Any Fermi level shift or DOS broadening may thus bring the γ value close to the experimental value $\approx 30\,\mathrm{mJ/mol\,K^2}$.

Studies of the volume dependence show that compressing below 90% of the experimental lattice parameter a_0 leads to a fast collapse of both spin and orbital moments of α-UH_3. Before this limit is reached, the orbital moments are reduced faster with pressure than the spin moments. The dramatic decrease starts at a values corresponding to $d_{\mathrm{U\text{-}U}}$ lower than the Hill limit 340 pm, and the $d_{\mathrm{U\text{-}U}}$ values around 300 pm, corresponding to weakly paramagnetic γ-U, still allow for small magnetic moments. The same type of calculation for γ-U at its experimental volume (i.e., α-UH_3 without hydrogen) yields a nonmagnetic state.

It would be interesting to find out whether the lower pressure sensitivity of spin moments comparing to orbital moments in U-based systems is a real phenomenon. As the spin magnetism originates naturally from band models, orbital magnetism has been perceived as a fingerprint of certain localization, and it should be therefore faster afflicted by pressure driven delocalization. Neutron form factor studies indeed indicate lower $|\mu_l/\mu_s|$ values for more delocalized actinide systems [36]. On the other hand, substantial orbital susceptibility has to be considered, due to the strong spin-orbit interaction, aside the spin susceptibility even in wide-band U systems, such as U metal [37]. The situation is not clear yet, partly because there is not yet a consensus about which computational method (different varieties of LDA + U and LSDA with orbital polarization) is more appropriate for different situations. An instructive discussion of the situation for U alloys can be seen, e.g., in Refs. [38,39].

On the quantitative level, we face an apparent disagreement between U moments of $1\,\mu_B$ and moments almost zero obtained from calculations. The fact that the total moment is obtained as a difference between antiparallel spin and orbital moments, being themselves much higher, makes the discrepancy merely quantitative, not qualitative. The picture can be modified, e.g., if orbital polarization is included. In such case, the orbital moments can be more pronounced [40].

Another issue, which could be addressed by computations, is whether the relative insensitivity of electronic properties to Zr alloying, which is unusual in band magnetics, can be understood by *ab initio* techniques. For the theoretical study of the effect of Zr alloying on magnetism of bcc U-based systems we employed the tight-binding linear muffin-tin orbital (TB-LMTO) method in the atomic-sphere approximation (ASA) combined with the coherent-potential approximation (CPA) for an efficient treatment of substitutionally disordered alloys [41–43]. We have studied the random binary $U_{1-x}Zr_x$ alloys with Zr concentrations $x < 0.5$ on a bcc lattice with the lattice parameter equal to that of bcc UH_3 ($a = 416\,\mathrm{pm}$). Using this crude model neglecting the role of hydrogen but allowing focusing on the substitution of U by Zr makes it computationally more tractable. In addition, we have studied not only the ferromagnetic state of the alloys, corresponding to their ground state, but also the so-called disordered-local-moment (DLM) state featured by randomly oriented U moments, which is relevant for the paramagnetic state [44]. This state has been simulated by a pseudoternary random alloy $(U^{+}_{0.5}U^{-}_{0.5})_{1-x}Zr_x$, where U^{+} and U^{-} denote, respectively, U atoms with two different orientations of their magnetic moments. The obtained values of the magnetic moments of U atom in both states are plotted in Fig. 11.

One can see that the large negative orbital moment of U is very stable with respect to Zr alloying. The positive spin magnetic moment in the ferromagnetic state depends slightly on the Zr concentration, but the spin moment in the DLM state is very stable again. It should be noted that the Zr atom in the ferromagnetic alloys exhibits a positive spin moment, in contrast to the DLM state where it is quenched completely, testifying that Zr moments are induced by the ferromagnetic order in the U subsystem. The stability of U moments in the binary U-Zr alloys is quite surprising having in mind the absence of magnetic order in pure metallic Zr. The stability of U moments seems to be related to the observed weak concentration dependence of the Curie temperature of the ternary $(UH_3)_{1-x}Zr_x$ system (Table I). However, the theoretical investigation of finite-temperature magnetic properties goes beyond the scope of the present work.

The comparison of U moments between the ferromagnetic and DLM state reveals that the moments are actually reversed. While the spin moment dominates in the ferromagnetic state (the correct value $\mu_U = 1.0\,\mu_B$ is most likely fortuitous), the insensitivity of the orbital moment to the spin disorder state

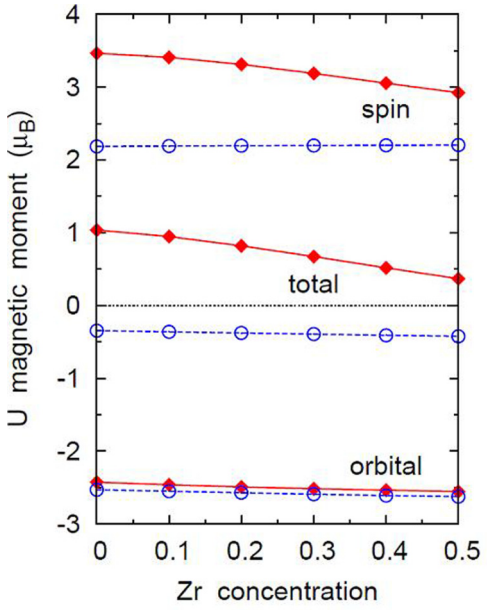

FIG. 11. (Color online) Calculated spin, orbital, and total magnetic moments of U atoms in a random bcc $U_{1-x}Zr_x$ alloy (with expanded volume) as functions of Zr concentration in the ferromagnetic (full diamonds) and the disordered-local-moment (DLM, open circles) states.

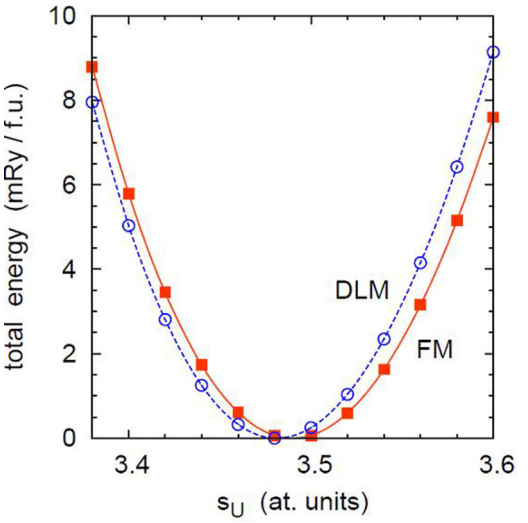

FIG. 12. (Color online) Calculated total energies (per formula unit) of hypothetical bcc UH_3 as functions of the Wigner-Seitz radius s_U of U atom in the ferromagnetic (FM, full squares) and disordered-local-moment (DLM, open circles) states. The experimental lattice parameter ($a = 416$ pm) corresponds to the value of $s_U = 3.47$ atomic units (1 atomic unit equals to the Bohr radius $a_B = 52.92$ pm). The curves are shifted vertically to have the minimum at the same energy, taken as zero on the vertical axis. The total energy minimum of the DLM state comes out by 1.5 mRy/f.u. above that of the FM state.

makes the orbital moment dominant in the paramagnetic state. As there is no systematic information on U orbital moments in the DLM state (the DLM approach was used for actinides in the context of phase stability studies [40]) we cannot be conclusive as to the relevance of the calculated orbital moments in the DLM state.

For assessment of the magnetovolume effects in the $(UH_3)_{1-x}Zr_x$ system, especially of its large observed spontaneous magnetostriction, we have employed the same approach as in the case of systems containing transition and rare-earth metals [45–47]. This approach rests on a treatment of the magnetically ordered state (ground state) and of the DLM state (paramagnetic state) and on the different equilibrium lattice parameters (alloy volumes) in these states, which give rise to the spontaneous volume magnetostriction. In the case of bcc UH_3, we applied the TB-LMTO-CPA method to a simplified model, containing one formula unit in the atomic basis on the bcc Bravais lattice: besides the sites of the bcc lattice occupied by U atom, six tetrahedral interstitial sites (per one U site) of the bcc lattice are randomly occupied by H atoms and vacancies (atoms with atomic number $Z = 0$) with probability 1/2, so that the total chemical composition of the model coincides with the real system. The calculations were confined to the scalar-relativistic approximation (neglecting the spin-orbit interaction). The valence basis comprises *spdf* orbitals of U atoms while only *sp* orbitals have been attached to H atoms and vacancies. The ratio of the Wigner-Seitz radii of the H and U spheres has been taken as $s_H/s_U = 0.4$. The volume dependence of the total energies of both magnetic states is displayed in Fig. 12. One can clearly see that the DLM state is featured by a slightly reduced equilibrium lattice parameter comparing to the ferromagnetic state; the calculated equilibrium properties are summarized in Table III. The equilibrium lattice parameter in the ferromagnetic state agrees reasonably well with the measured value and with the theoretical value calculated by the more accurate fully relativistic technique (see above), while the bulk modulus comes out significantly higher than in experiment, in line with other calculations. The relative difference of the lattice parameter in the two magnetic states can be (after multiplication by the factor of 3) identified with the spontaneous volume magnetostriction. Its calculated value amounts to $\omega_s = 7.5 \times 10^{-3}$, which represents a large effect, being of a similar magnitude as the measured value ($\omega_s = 3.2 \times 10^{-3}$). The origin of this large positive magnetostriction can be, in analogy to the transition-metal and rare-earth-metal systems, ascribed mainly to the reduction of the spin magnetic moment in the DLM state as compared to the ferromagnetic state: the spin moment of U is reduced by about 10% due to the magnetic disorder (see Table III). The obtained semiquantitative agreement between the theoretical and measured spontaneous magnetostriction corroborates the itinerant

TABLE III. Values of equilibrium lattice parameter a, bulk modulus B, spin magnetic moment of U atom m_U and total spin moment per formula unit M in the ferromagnetic (FM) and the disordered-local-moment (DLM) states of hypothetical bcc UH_3 (see the text for details) as obtained from scalar-relativistic TB-LMTO-CPA calculations.

State	a (pm)	B (GPa)	m_U (μ_B)	M (μ_B)
FM	417.99	109	2.14	2.24
DLM	416.95	116	±1.94	0

nature of magnetism of the UH_3 system; a more accurate theoretical description, including the effect of spin-orbit interaction and of Zr alloying, remains the task for future studies.

IV. DISCUSSION AND CONCLUDING REMARKS

The new and well established data on α-UH_3 complement interesting but fragmentary information on U hydrides in general. The relatively very high T_C values (in the context of actinide magnetism) of β-UH_3 has not been perceived as anomalous, because it was actually the first pure $5f$ ferromagnet discovered. It was preceded only by UFe_2 [48], in which similar $T_C = 160\,K$ [49] is mainly due to the involvement of Fe-$3d$ states. The β-UH_3 type compounds, U_6FeH_{17} and U_6CoH_{18} [11,12] have been taken simply as analogs of β-UH_3. Our discovery of U hydrides with amorphous or α-UH_3 structure, which all exhibit similar ordering temperatures and U moments around $1\,\mu_B$ as well as the Sommerfeld coefficient $\approx 30\,mJ/mol\,K^2$ bring up the question about the reason for such uniformity in a material, assumed to be an itinerant $5f$-ferromagnet, while the band $5f$ states in light actinides are normally very sensitive to all variables. Certain hints seem to be provided by the preliminary electronic structure calculations presented in this work. The shift of the electronic states of uranium to higher energies is applicable to U-$6d$ and $7s$ states only, and the $5f$ states remaining below the Fermi energy have less opportunity to hybridize with non-f states. In such situation, the Hill limit of 340 pm [4], which was empirically determined assuming a number of intermetallics with hybridized $5f$ states, has to be "renormalized" and the critical U-U spacing needed for magnetic ground state must be much smaller. More systematic work using various computational methods would bring more quantitative understanding.

The calculations performed so far (ours or in Ref. [31]) exhibit a certain disagreement with the high-resolution UPS data [50], which show the occupied part of the $5f$ band in UH_3 to almost 2 eV binding energy exceeding thus the calculated DOS not reaching more than 1 eV binding energy. More advanced calculations using LDA + U, LDA+Hubbard I, or DMFT should determine whether the ground-state DOS is modified if the e-e correlations are treated more explicitly or whether it is actually the f^2 final-state multiplet appearing in the valence-band spectra, as suggested in Ref. [50], stressing possible similarities with NpH_3 and PuH_3.

An important feature of the $5f$ magnetism in UH_3 is the sizeable orbital moment revealed by the calculations, which is a necessary ingredient of high magnetic anisotropy. The fact that light actinides have large orbital moments (antiparallel to spin moments due to strong spin-orbit interaction) despite the band character of the $5f$ states was pointed out by Brooks and Kelly [51]. Our LSDA calculations give only semiquantitative prediction of the magnitude of spin and orbital moments, but existence of sizeable orbital moments cannot be doubted. The related anisotropy is explaining the high coercivity and slow approach to saturation of magnetization in high fields. Orbital effects in $5f$-band ferro- or antiferromagnets have been naturally more visible in the bulk properties in the case of low symmetry structures [21]. Macroscopic studies of cubic materials do not reveal such a striking anisotropy due to possible higher multiplicities of easy-magnetization direction, but it does not mean that the anisotropy energy must be lower. The determination of the U moment direction (easy magnetization direction) is a task for future experiments. Those experiments may benefit from the fact that while the alloyed UH_3 hydrides have very similar properties to their pure precursors, their stability (resistance to oxidation and mechanical decrepitation) is much better and even monolithic pieces can be used.

At present, the main reason for this stability is not clear. The decrepitation of U metal upon hydrogenation can be associated with the very low solubility of H in α-U. The absence of a solid solution of H in U, representing an intermediate step in hydrogenation, makes the volume increase to UH_3 so dramatic and abrupt, forming a sharp interface between U and UH_3, proceeding fast inwards. The solubility of H in γ-U is much higher [52], which makes the interface wider and perhaps better accommodating mechanical strains. We may assume that substituted bcc U alloys retain this feature.

The fact that high H pressures are needed for hydrogenation of alloyed bcc U can be due to either thermodynamic (different enthalpy of formation) or kinetic (difference in H diffusion, passivation of surface by segregated dopants) reasons. A surface science study is planned to explain this effect, which makes U hydrides much more user friendly materials.

ACKNOWLEDGMENTS

This work was supported by the Czech Science Foundation under the Grant Nos. P204/12/0285, P204/10/0330 and 15–01100S. M. Paukov was supported by the Grant Agency of the Charles University under the project No. 1332314. Experiments were partly performed at MLTL (http://mltl.eu/), which is supported within the program of Czech Research Infrastructures (project No. LM2011025). Participation N.-T.H.K-N. was supported by the program MOBILITY 7AMB14PL036 (Czech-Polish bilateral cooperation).

[1] C. Ablitzer, F. Le Guyadec, J. Raynal, X. Génin, and A. Duhart-Barone, J. Nucl. Mater. **432**, 135 (2013).
[2] R. Troc and W. Suski, J. Alloys Comp. **219**, 1 (1995).
[3] J. W. Ross and D. J. Lam, Phys. Rev. **165**, 617 (1968).
[4] H. H. Hill, in *Plutonium 1970 and Other Actinides*, edited by W. N. Miner (AIME, New York, 1970), pp. 1–19.
[5] S. Doniach, Physica B **91**, 231 (1977).
[6] L. Havela, A. Shick, and T. Gouder, J. Appl. Phys. **105**, 07E130 (2009).
[7] J. H. Shim, K. Haule, and G. Kotliar, Nature (London) **446**, 513 (2007).
[8] D. D. Koelling, B. D. Dunlap, and G. W. Crabtree, Phys. Rev. B **31**, 4966 (1985).
[9] I. Tkach, N. T. H. Kim-Ngan, A. Warren, T. Scott, A. P. Gonçalves, and L. Havela, Physica C **498**, 14 (2014).

[10] V. Sechovsky and L. Havela, in *Handbook of Magnetic Materials*, Vol. 4, edited by E. P. Wohlfarth and K. H. J. Buschow (Elsevier, Amsterdam, 1988), pp. 309–491.

[11] H. Drulis, F. G. Vagizov, M. Drulis, and T. Mydlarz, Phys. Rev. B **52**, 9500 (1995).

[12] A. V. Andreev, M. I. Bartashevich, A. V. Deryagin, L. Havela, and V. Sechovsky, Phys. Stat. Sol. A **98**, K47 (1986).

[13] Ch. D. Taylor, T. Lookman, and R. S. Lillard, Acta Materialia **58**, 1045 (2010).

[14] I. Grenthe, J. Drozdynski, T. Fujino, E. C. Buck, T. E. Albrecht-Schmitt, and S. F. Wolf, in *The Chemistry of the Actinide and Transactinide Elements*, 3rd ed., edited by J. J. Katz, J. R. Morss, N. Edelstein, and J. Fuger (Springer, Dordrecht, 2006), pp. 253–698.

[15] A. C. Lawson, J. A. Goldstone, J. G. Huber, A. L. Giorgi, J. W. Conant, A. Severing, B. Cort, and R. A. Robinson, J. Appl. Phys. **69**, 5112 (1991).

[16] I. Tkach, S. Mašková, Z. Matěj, N.-T. H. Kim-Ngan, A. V. Andreev, and L. Havela, Phys. Rev. B **88**, 060407(R) (2013).

[17] L. Havela, M. Paukov, I. Tkach, Z. Matej, N.-T. H. Kim-Ngan, and A. V. Andreev, in *2014 MRS Spring Meeting - Basic Science, Applications and Technology*, Materials Research Society Symposium Proceedings Vol. 1683 (Materials Research Society, Pittsburgh, 2014), mrss14-1683-s03-02.

[18] G. C. Hajipanayis, J. Magn. Magn. Mater. **200**, 373 (1999).

[19] T. Egami, Phys. Stat. Sol. A **19**, 747 (1973); **20**, 157 (1973).

[20] H. Oesterreicher, F. T. Parker, and M. Misroch, Phys. Rev. B **18**, 480 (1978).

[21] L. Havela, V. Sechovský, F. R. de Boer, E. Brück, and H. Nakotte, Physica B **177**, 159 (1992).

[22] M. S. Henriques, D. I. Gorbunov, J. C. Waerenborgh, L. Havela, A. B. Shick, M. Diviš, A. V. Andreev, and A. P. Gonçalves, J. Phys.: Condens. Matter **25**, 066010 (2013).

[23] A. Wallash, J. Crow, and Z. Fisk, J. Appl. Phys. **57**, 3143 (1985).

[24] P. Javorský, L. Havela, F. Wastin, P. Boulet, and J. Rebizant, Phys. Rev. B **69**, 054412 (2004).

[25] V. Sechovský, L. Havela, G. Hilscher, N. Pillmayr, A. V. Andreev, P. A. Veenhuizen, and F. R. de Boer, J. Appl. Phys. **63**, 3070 (1988).

[26] A. V. Andreev, S. M. Zadvorkin, M. I. Bartashevich, T. Goto, J. Kamarád, Z. Arnold, and H. Drulis, J. Alloys Comp. **267**, 32 (1998).

[27] I. Y. Glagolenko, K. P. Carney, S. Kern, E. A. Goremychkin, T. J. Udovic, J. R. D. Copley, and J. C. Cook, Appl. Phys. A **74** (Suppl.), S1397 (2002).

[28] J. C. Fernandes, M. A. Continentino, and A. P. Guimaraes, Solid State Commun. **55**, 1011 (1985).

[29] J. W. Ward, L. E. Cox, J. L. Smith, G. R. Stewart, and J. H. Wood, J. Physique **40** (Suppl. 4), 15 (1979).

[30] A. C. Switendick, J. Less Common Met. **88**, 257 (1982).

[31] Ch. D. Taylor, Phys. Rev. B **82**, 224408 (2010).

[32] I. Halevy, S. Salbov, S. Zalkind, M. Brill, and I Yaar, J. Alloys Comp. **370**, 59 (2004).

[33] Y. Zhang, B. Wang, Y. Lu, Y. Yang, and P. Zhang, J. Nucl. Mater. **430**, 137 (2012).

[34] K. Koepernik and H. Eschrig, Phys. Rev. B **59**, 1743 (1999).

[35] J. P. Perdew and Y. Wang, Phys. Rev. B **45**, 13244 (1992).

[36] B. Lebech, M. Wulff, and G. H. Lander, J. Appl. Phys. **69**, 5891 (1991).

[37] A. Hjelm, J. Trygg, O. Eriksson, B. Johansson, and J. Wills, Phys. Rev. B **50**, 4332 (1994).

[38] W. Xie, W. Xiong, C. A. Marianetti, and D. Morgan, Phys. Rev. B **88**, 235128 (2013).

[39] P. Söderlind, A. Landa, and P. E. A. Turchi, Phys. Rev. B **90**, 157101 (2014).

[40] J. R. Jeffries, P. Söderlind, H. Cynn, A. Landa, W. J. Evans, S. T. Weir, Y. K. Vohra, and G. H. Lander, Phys. Rev. B **87**, 214104 (2013).

[41] I. Turek, V. Drchal, J. Kudrnovský, M. Šob, and P. Weinberger, *Electronic Structure of Disordered Alloys, Surfaces and Interfaces* (Kluwer, Boston, 1997).

[42] A. B. Shick, V. Drchal, J. Kudrnovský, and P. Weinberger, Phys. Rev. B **54**, 1610 (1996).

[43] I. Turek, J. Kudrnovský, and K. Carva, Phys. Rev. B **86**, 174430 (2012).

[44] B. L. Gyorffy, A. J. Pindor, J. Staunton, G. M. Stocks, and H. Winter, J. Phys. F: Met. Phys. **15**, 1337 (1985).

[45] S. Khmelevskyi, I. Turek, and P. Mohn, Phys. Rev. Lett. **91**, 037201 (2003).

[46] S. Khmelevskyi, I. Turek, and P. Mohn, Phys. Rev. B **70**, 132401 (2004).

[47] I. Turek, J. Rusz, and M. Diviš, J. Alloys Comp. **431**, 37 (2007).

[48] P. Gordon, Ph.D. thesis, Massachusetts Institute of Technology, Cambridge, MA, 1949.

[49] A. T. Aldred, J. Magn. Magn. Mater. **10**, 42 (1979).

[50] T. Gouder, A. Seibert, J. Rebizant, F. Huber, and L. Havela, in *Actinides 2006 - Basic Science, Applications and Technology*, Materials Research Society Symposium Proceedings Vol. 986 (Materials Research Society, Pittsburgh, 2007), pp. 17–28.

[51] M. S. S. Brooks and P. J. Kelly, Phys. Rev. Lett. **51**, 1708 (1983).

[52] Binary Alloy Phase Diagrams, ASM International, 1980.